# Local solubility of nonpolar molecules in the liquid–vapor interfaces of water and simple liquids

**ARTICLE** *in* JOURNAL OF MOLECULAR LIQUIDS · DECEMBER 2014

Impact Factor: 2.52 · DOI: 10.1016/j.molliq.2014.02.014



**2 AUTHORS**, INCLUDING:

Kenichiro Koga

Okayama University

**73** PUBLICATIONS **2,088** CITATIONS

SEE PROFILE

Journal of Molecular Liquids 200 (2014) 7–11

Contents lists available at ScienceDirect

Journal of Molecular Liquids

journal homepage: www.elsevier.com/locate/molliq

# Local solubility of nonpolar molecules in the liquid–vapor interfaces of water and simple liquids

K. Abe, K. Koga *

*Department of Chemistry, Faculty of Science, Okayama University, Tsushima-Naka 3-1-1, Okayama 700-8530, Japan*

ARTICLE INFO

*Article history:*
Received 6 November 2013
Received in revised form 2 January 2014
Accepted 17 February 2014
Available online 6 March 2014

*Keywords:*
Hydrophobic
Lennard–Jones
Surface
Adsorption

ABSTRACT

The local solubility $\Sigma$ of nonpolar molecules at the liquid–vapor interface is examined for model systems of water and simple liquids. For Lennard–Jones (LJ) solutes in model water and those in the LJ solvent, $\Sigma$ is obtained by the Widom test particle method as a function of the coordinate normal to the interface. In order to examine the effect of the solvent structure on $\Sigma$, we compare the dependence of $\Sigma$ on a reduced coarse-grained density of the solvent $\rho_{cg}^{*}$ for water with that for the LJ solvent under the condition that $\varepsilon/T$ is common for the two systems, where $\varepsilon$ is the LJ energy parameter between solute and solvent molecules and $T$ is the temperature. We found that the solubility $\Sigma$ of the LJ solute is higher in water than in the LJ solvent at any given $\rho_{cg}^{*}$, i.e., structure of water has higher ability to dissolve the nonpolar molecule than that of simple liquids, not only in their liquid states but also in their interfacial regions. This is partly because the probability of forming a sufficiently large cavity is higher in water than in the LJ fluid, as confirmed by the calculation of the local solubility of the hard-sphere solute. In addition, it is found that variation of the probability of cavity formation with $\rho_{cg}$ in water is very similar to that in the LJ solvent if $\rho_{cg}$ is scaled with the bulk liquid density.



## 1. Introduction

Much attention has been paid to the behavior of solute molecules at the liquid–vapor interface, where the density of solvent varies rapidly within a distance of few molecular diameters [1–8]. Surface-specific spectroscopic techniques, such as second-harmonic generation (SHG) and sum-frequency generation (SFG) [2,3,9], are used to investigate solute molecules adsorbed at interfaces. Application of these methods ranges from investigating the orientation and the hydration structure of small molecules at the air–water interface [10–13] to detecting the structure and phase transitions in a dense monolayer of surfactant at the interface [1,14–16]. However, the spacial distribution of solute species in the interface has not been determined from experiments.

Molecular-scale information on the solvation in the liquid–vapor interface can be obtained by computer simulation [4–8,17]. A fundamental question is how the solubility of a solute varies with the height $z$ through an interface. The spacial dependence of the solubility can be described by the excess chemical potential $\mu_{ex}$ of the solute as a function of $z$. There are many studies on the calculation of $\mu_{ex}(z)$ of various molecules in the liquid–vapor interface of water [18–23]. The common behavior of $\mu_{ex}(z)$ obtained for hydrophobic solutes is as follows: (i) it has a minimum at the interface, i.e., solutes are surface active; (ii) its value at the bulk liquid phase is very high, i.e., the solubility in the bulk water is very small; and (iii) there is a free energy barrier around the liquid-side of the interface.

The solvation in the liquid–vapor interface of simple fluids is not well studied [24] as compared to that of water. For example, the profiles of $\mu_{ex}(z)$ are still unknown for nonpolar, monatomic gases at the interface. One of the purposes of the present study is to examine whether or not the behavior of $\mu_{ex}(z)$ of hydrophobic solutes in the interface of water is qualitatively different from that in the interface of simple liquids.

An intuitive understanding of the solvation at infinite dilution is gained by the Widom test-particle theory [25–27]. At infinite dilution, the excess chemical potential of a solute at position $\mathbf{r}$ in a solvent is expressed as an average of the Boltzmann factor $e^{-\Psi/kT}$ over the canonical ensemble of the solvent

$$\mu_{ex}(\boldsymbol{r}) = -kT \ln \left\langle e^{-\Psi(\boldsymbol{r})/kT} \right\rangle, \tag{1}$$

where $T$ is the temperature and $k$ is Boltzmann's constant. $\Psi(\boldsymbol{r})$ is the interaction energy of the test particle (solute molecule) fixed at $\boldsymbol{r}$ with all solvent molecules. When the test particle overlaps with any one of solvent molecules, the solute–solvent interaction energy is infinitely high, and then the Boltzmann factor is essentially zero. For the Boltzmann factor to be nonzero, a cavity larger than the size of the solute molecule has to be formed at $\mathbf{r}$. If the cavity is sufficiently large, the Boltzmann factor is greater than 1, for then the solute–solvent attractive interactions make $\Psi$ less than 0. The strength of attraction increases with the number of solvent molecules in the vicinity of the cavity. Thus, there are two aspects of the structure of solvent which are

* Corresponding author.

http://dx.doi.org/10.1016/j.molliq.2014.02.014
0167-7322/

relevant to the solubility of nonpolar solutes. One is the probability of cavity formation and the other is the coordination number of the solvent molecules around the cavity.

Another factor that affects the solubility is a pair interaction energy between solute and solvent molecules divided by $kT$. Let us compare methane in water with methane in krypton, both near the triple point. With the Lennard–Jones (LJ) energy parameter $\varepsilon_{AB}$ chosen for the two systems [28,29], one finds that $\varepsilon_{AB}/kT \sim 0.4$ for methane in water and ~1.3 for methane in krypton. In part, this difference explains the low solubility of methane in water as compared to that of methane in krypton. Therefore, both the effect of solvent structure and that of the characteristic pair interaction energy divided by $kT$ should be considered, when local solubilities of various systems are compared.

We compare the solubility profiles of small, nonpolar molecules in the liquid–vapor interface of water with that in the interface of the LJ liquid. For both systems, the solute–solvent interaction is described by the LJ potential, that is, the solute is the LJ particles. The density profile of solvent molecules is obtained by molecular dynamics simulation and $\mu_{ex}(z)$ is calculated by the Widom test particle method as in previous studies [20,30–32].

In order to clarify the effect of the solvent structure on the local solubility, we present the results and analyses in the following order. First, we compare behavior of $\mu_{ex}(z)$ in water with that in the LJ solvent under the condition that the reduced solute–solvent LJ parameters $\sigma^*$ and $\varepsilon^*$ are common for the two systems and the temperature is close to the triple point of each solvent. The $\sigma^*$ and $\varepsilon^*$ are the solute–solvent LJ parameters $\sigma_{AB}$ and $\varepsilon_{AB}$ divided by the solvent–solvent LJ parameters $\sigma_{BB}$ and $\varepsilon_{BB}$, respectively. Second, we express $\mu_{ex}$ as functions of a solvent density which varies through the interface and compare $\mu_{ex}$ for water with that for the LJ fluid. This enables us to examine the difference in $\mu_{ex}$ between the two systems eliminating the contribution from the density difference. Third, we make the same comparison under the condition that $\varepsilon_{AB}/kT$ is common for the two systems. Then we may examine the difference in $\mu_{ex}$ that arises only from the difference in solvent structure. Finally, we also compare the probability of cavity formation in the interface of water with that in the interface of the LJ solvent. The present calculation suggests that the probability of cavity formation in the liquid–vapor interface is a universal function of a solvent density scaled by that of the coexisting liquid phase.

## 2. Theory

Suppose that the system is composed of $N_A$ solute and $N_B$ solvent molecules in a fixed volume $V$, that it is in a state of the liquid–vapor coexistence, and that the solute and solvent local densities $\rho_A$ and $\rho_B$ vary only in one direction. Let the $z$-axis be in that direction, which is normal to the liquid–vapor interface, with $z < 0$ in the gas phase, $z > 0$ in the liquid phase, and $z = 0$ at the Gibbs equimolar dividing surface [33] for the solvent density. This mathematical surface divides $V$ into $V^g$ and $V^l$, volumes of the gas and liquid regions, in the way the following condition is satisfied:

$$\rho_B^g V^g + \rho_B^l V^l = N_B, \tag{2}$$

where $\rho_B^g$ and $\rho_B^l$ are the solvent densities of the homogeneous gas and liquid phases at the two-phase equilibrium.

In what follows, we consider infinitely-dilute solutions: $N_A/V \to 0$. Let us define the local solubility $\Sigma(z)$ at the position $z$ by

$$\Sigma(z) = \frac{\rho_A(z)}{\zeta_A}, \tag{3}$$

where $\zeta_A$ is the activity of the solute defined such that $\zeta_A \to \rho_A$ as $\rho_A \to 0$ and $\rho_B \to 0$. Then, $\Sigma(z) \simeq 1$ in the homogeneous gas phase ($z \to -\infty$) and $\Sigma(z) \simeq \rho_A^l/\rho_A^g$ in the homogeneous liquid phase ($z \to +\infty$), the latter of which is the equilibrium ratio of the solute density in the liquid phase to that in the gas phase (the Ostwald adsorption coefficient). The local excess chemical potential $\mu_{ex}(z)$ is related to $\Sigma(z)$ via $\mu_{ex}(z) = -kT \ln \Sigma(z)$.

The activity $\zeta_A$ of the solute at infinite dilution is by definition

$$\zeta_A = \frac{Q_0}{Q_1}, \tag{4}$$

where $Q_0$ and $Q_1$ are the configurational integrals of the system with $N_A = 0$ (system 0) and the system with $N_A = 1$ (system 1), respectively. Note that $\zeta_A$ is uniform throughout the system as are the chemical potential $\mu_A$ and the temperature $T$. Let $\Psi(r) = \Psi\left(r, r_1, \ldots, r_{N_B}\right)$ be the interaction energy of the solute molecule at $r$ with $N_B$ solvent molecules at $r_1, \ldots, r_{N_B}$ and $U_0 = U_0\left(r_1, \ldots, r_{N_B}\right)$ and $U_1(r) = U_1\left(r, r_1, \ldots, r_{N_B}\right)$ be the potential energies of system 0 and that of system 1, respectively. Noting that $U_1(r) = \Psi(r) + U_0$, Eq. (4) is now written

$$\zeta_A = \frac{\frac{1}{Q_1}\int exp(-U_1(r)/kT)\mathrm{d}r^{N_B}}{\frac{1}{Q_0}\int exp(-\Psi(r)/kT)exp(-U_0/kT)\mathrm{d}r^{N_B}} = \frac{\rho_A(r)}{\langle exp(-\Psi(r)/kT)\rangle}, \tag{5}$$

where $<\ldots>$ means the average with the factor $\exp(-U_0/kT) / Q_0$ over the coordinates of solvent molecules (i.e., the average over the configuration in system 0) and $\rho_A(r)$ is the local density of solute at position r in system 1. Since the system is homogeneous in any plane normal to the $z$ axis, the numerator and denominator are functions of $z$ alone. The local solubility defined in Eq. (3) is then

$$\Sigma(z) = \langle \exp(-\Psi(z)/kT)\rangle. \tag{6}$$

This is the potential distribution theorem for inhomogeneous systems [27] and what we will use for calculating the local solubility $\Sigma(z)$ of solutes through the liquid–vapor interface of the model systems described below.

## 3. Methods

We consider two model solvents: the TIP4P/2005 model water [29] and the LJ solvent. Each molecule of the model water has one LJ interaction site on the oxygen atom with the size and energy parameters $\sigma_{BB} = 3.1589$ Å and $\varepsilon_{BB}/k = 93.2$ K and three Coulomb interaction sites. In both solvents, the pair interaction between solvent and nonpolar-solute molecules is taken to be the LJ potential function and the LJ parameters, $\sigma_{AB}$ and $\varepsilon_{AB}$, are varied in order to examine the effects of the solute size and the strength of solute–solvent attraction on the local solubility.

To obtain equilibrium configurations of the liquid–vapor interface, we carried out the NVT-ensemble molecular dynamics simulation of the model water and the LJ solvent. The program package GROMACS 4.5.5 [34] was employed for the model system of pure water and our own MD program was used for the LJ solvent. The simulation cell is a rectangular box ($L_x = L_y < L_z$) and contains 1372 solvent molecules under the periodic boundary conditions in the three directions. The temperature is fixed at $T = 273$ K for water and $T^* = kT/\varepsilon_{BB} = 0.7$ for the LJ solvent using the Nosé [35] or Nosé–Hoover [36,37] thermostat. The initial configuration is prepared by placing a dense-liquid slab of molecules in the middle of the rectangular cell. The configuration is sampled every 100 steps after the equilibration period of $1 \times 10^6$ steps. There are two liquid–vapor interfaces in each equilibrium configuration.

In the simulation of pure water, we set $L_x = L_y = 37.15$ Å and $L_z = 111.5$ Å. Both the Coulomb and LJ parts of the intermolecular interaction are smoothly truncated between 12 and 13 Å using a switching function. The Coulomb interaction is treated by the particle mesh Ewald method. The time step is 1 fs. For the LJ solvent, the simulation box has the dimensions $L_x = L_y = 11.76\sigma_{BB}$ and $L_z = 35.29\sigma_{BB}$. The LJ interaction is gradually switched off between 3.91 $\sigma_{BB}$ and 4.50 $\sigma_{BB}$.

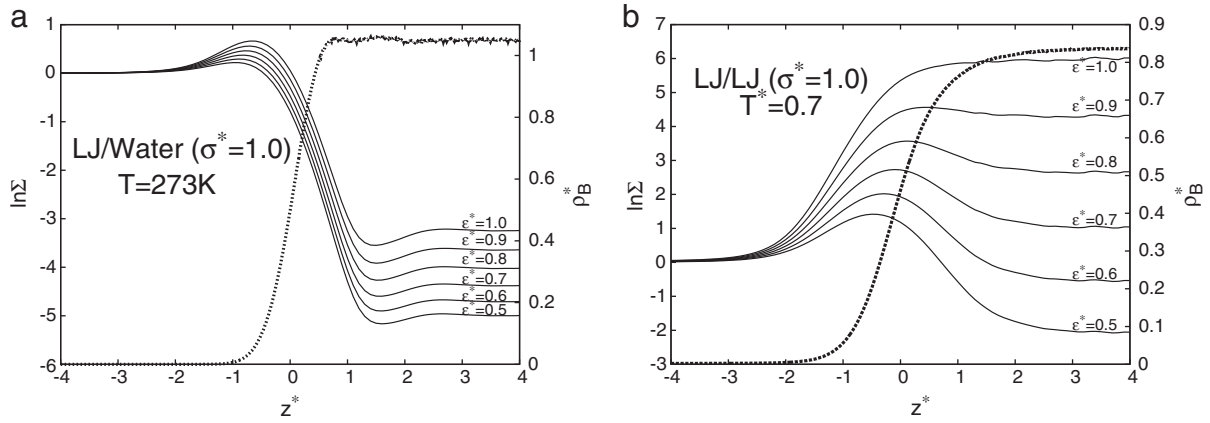


**Fig. 1.** The local solubility of LJ solutes in the logarithmic scale $\ln\Sigma(z^*)$ (solid lines) and the reduced density profile $\rho_B^*(z^*)$ of the solvent (dashed line) for (a) water at $T = 273$ K and (b) the LJ solvent at $T^* = 0.7$. The reduced coordinate $z^* = z/\sigma_{BB}$ and $\rho_B^*(z^*) = \sigma_{BB}^3\rho_B(z^*)$. The $z^* = 0$ is the Gibbs equimolar surface.

The dimensionless time-step $\Delta t^* = \Delta t\sqrt{\varepsilon_{BB}}/(\sigma_{BB}\sqrt{m})$ is chosen to be $4.6 \times 10^{-4}$, where $m$ is the mass of the particle.

The equilibrium configurations of the solvents obtained by simulation are used for the particle insertion calculation. Before performing the particle insertion, we calculate the Gibbs equimolar dividing surface every $2 \times 10^5$ steps to redefine the origin of the $z$-axis. This procedure is essential to ensure that the relative distance between the test particle and the dividing surface is invariant for each insertion; otherwise, $\Sigma(z)$ would be undesirably broadened due to the translational motion of the interface in the course of simulation. The test particle (solute molecule) is inserted into $70 \times 70$ lattice points on the plane of constant $z$ defined with respect to each interface: note that there are two interfaces in the system. The total number of the trial insertions at each $z$ in the set of equilibrium configurations is about $5 \times 10^9$. The local solubility $\Sigma(z)$ is then obtained by varying $z$ with an interval of 0.10 $\sigma_{BB}$.

## 4. Results

### 4.1. Behavior of $\Sigma(z)$ near the triple point

In Fig. 1, we show the local solubility (in the logarithmic scale) of LJ solutes (a) in water at $T = 273$ K and (b) in the LJ solvent at $T^* = 0.7$, together with the reduced local density $\rho_B^*(z^*) = \sigma_{BB}^3\rho_B(z^*)$ of the solvent, as functions of $z^* = z/\sigma_{BB}$. The thermodynamic state of the model systems is specified by temperature alone because the infinitely-dilute solutions (solvents) are one-component, two-phase systems. In both cases, the liquid, gas, and the interface examined here are in a state close to the triple point. The profiles $\ln\Sigma(z^*)$ in Fig. 1 are those obtained for six different solutes with the solute–solvent LJ parameters $\varepsilon^* = \varepsilon_{AB}/\varepsilon_{BB} = 0.5, 0.6, \ldots, 1$ and $\sigma^* = \sigma_{AB}/\sigma_{BB} = 1$.

Both in water and in the LJ solvent, $\ln\Sigma(z^*) \simeq 0$, or equivalently $\Sigma \simeq 1$, for the gas-phase region ($z^* < -3$). This is what we have anticipated earlier. In the case of water (Fig. 1a), $\ln\Sigma$ exhibits a local maximum on the vapor side of the interface (in a range $-1 < z^* < 0$) and a local minimum on the liquid side (in a range $1 < z^* < 2$) and varies rapidly in a narrow range including the equimolar surface $z^* = 0$. That $\ln\Sigma(z^*) < 0$ deep inside the liquid region indicates $\mu_{ex}(z^*) > 0$. The local maximum in $\ln\Sigma$ is equivalent to a local minimum in $\mu_{ex}(z^*)$: it is the manifestation of the interface adsorption of the solute. The local minimum in $\ln\Sigma$ means a local maximum in $\mu_{ex}(z^*)$, which has been observed as the free energy barrier in earlier works [6,18,21]. It is clear in Fig. 1a that $\ln\Sigma(z^*)$ at any fixed $z^*$ increases with increasing the solute–solvent LJ energy parameter $\varepsilon^*$.

In the LJ solvent, too, $\ln\Sigma(z^*)$ at any given $z^*$ increases as $\varepsilon^*$ increases. When $\varepsilon^* = 1.0$, i.e., the solute molecule is identical to the solvent molecule, there is no maximum in $\Sigma(z^*)$ whereas for all $\varepsilon^* \le 0.9$, the adsorption at interface is observed. With $\varepsilon^* \ge 0.7$, $\Sigma(z^*)$ in the liquid-phase region ($z^* \simeq 4$) is greater than 1, i.e., the solute molecule favors the liquid phase than the gas phase. This is in contrast to the case of water for which we found $\Sigma(z^* \simeq 4) < 1$ for all $\varepsilon^*$ examined. The LJ solute in the LJ solvent exhibits both the interface adsorption and the negative $\ln\Sigma(z^*)$ in the liquid-phase region if $\varepsilon^* \le 0.6$, that is, only if the solute–solvent attractive interaction is much weaker than the solvent–solvent one. On the other hand, LJ solutes in water exhibit both of the features even if $\varepsilon^*$ is as large as 1.5. However, this condition for water does not mean that the solute–solvent attractive

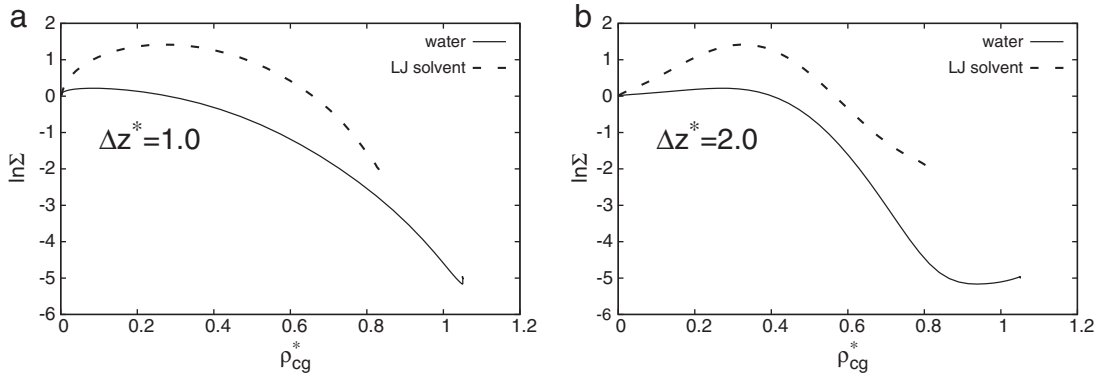


**Fig. 2.** Correlation between $\ln\Sigma$ of the LJ solute and the reduced coarse-grained solvent density $\rho_{cg}^*$ for water (solid line) and the LJ solvent (dashed line). The $\Delta z^*$ with which $\rho_{cg}^*$ is defined is (a) 1.0 and (b) 2.0. The solute–solvent LJ parameters are $z^* = 1.0$ and $\varepsilon^* = 0.5$ both for water and for the LJ solvent. The temperatures are the same as in Fig. 1.

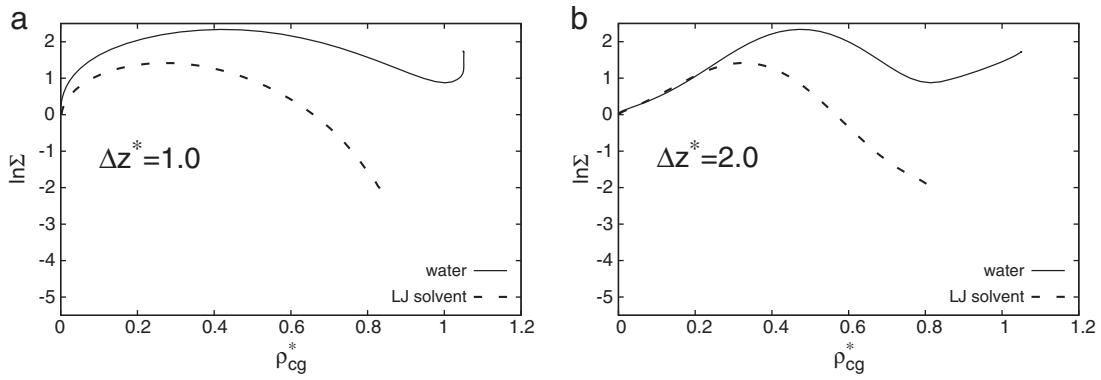


**Fig. 3.** Correlation between ln Σ of the LJ solute and the reduced coarse-grained solvent density $\rho^*_{cg}$. The value of $\varepsilon^*$ is chosen so that $\varepsilon^*/T^*$ is common for the two systems: for water $T^* = 2.929$ ($T = 273$ K) and $\varepsilon^* = 2.09$; for the LJ solvent $T^* = 0.7$ and $\varepsilon^* = 0.50$.

interaction is stronger than the solvent–solvent one because in the case of water a large part of the intermolecular attraction arises from the Coulomb interactions.

### 4.2. Effect of the solvent structure on the solubility

The local solubility $\Sigma(z)$ at given $z$ for water and that for the LJ solvent differ significantly even though both solvents are in states close to their triple points and both systems have the same solute–solvent pair potential function. A possible reason for the difference in $\Sigma(z)$ is difference in the reduced solvent density $\rho^*_B(z)$ at given $z$. To exclude this effect, we plot ln Σ against $\rho^*_{cg}$ in Fig. 2, where $\rho^*_{cg}$ is $\rho^*_B(z^*)$ averaged over a range $[z^* - \Delta z^*, z^* + \Delta z^*]$ and is referred to as the coarse-grained solvent density. Note that both ln Σ and $\rho^*_{cg}$ are functions of $z^*$ but now we examine how ln Σ changes with $\rho^*_{cg}$ as $z$ varies through the interface. Two choices of $\Delta z^*$ are employed for $\rho^*_{cg}$: $\Delta z^* = 1$ (Fig. 2a) and $\Delta z^* = 2$ (Fig. 2b). In either case, the local solubility in the LJ solvent is higher than that in water at any given $\rho^*_{cg}$ when the solute–solvent LJ parameters $\sigma^*$ and $\varepsilon^*$ are common and the temperature is close to the triple point.

Now we compare the plots of ln Σ vs $\rho^*_{cg}$ for the two solvents when $\sigma^*$ and $\varepsilon^*/T^* = \varepsilon_{AB}/kT$ are common. The reason we choose $\varepsilon^*/T^*$ to be common is that by doing so one may examine the effect of the solvent structure on Σ, excluding the effect of temperature. Under this condition we would find the same Σ if the solvent structures were the same for the two different systems with different temperatures, because the solubility Σ of the LJ solute is a function of $\sigma^*$ and $\varepsilon^*/T^*$. We have chosen $\varepsilon^* = 2.09$ for water and $\varepsilon^* = 0.50$ for the LJ solvent so that $\varepsilon^*/T^* = 5/7$, a common value for the two systems. Fig. 3 shows that in either choice of $\Delta z^*$, the solubility in water is higher than that in the LJ solvent. This is opposite to what we have found in Fig. 2. Nonpolar solutes (LJ particles) are more soluble in water than in the LJ solvent for any given solvent density $\rho^*_{cg}$ in the liquid–vapor interfacial region if the solute–solvent $\sigma^*$ and $\varepsilon^*/T^*$ are chosen to be common. Also, the solubility in bulk liquid water is higher than that in the bulk LJ liquid if $\sigma^*$ and $\varepsilon^*/T^*$ are common for the two systems. The latter is observed for other values of $\varepsilon^*/T^*$ (=6/7,7/7,…,15/7), too.

### 4.3. Difference in the probability of cavity formation between water and the Lennard–Jones solvent

In Section 4.2, we have seen that the model water with its liquid–vapor interface has higher ability to dissolve the LJ solute at given solvent density $\rho^*_{cg}$ than that of the LJ solvent with its interface under the condition that $\sigma^*$ and $\varepsilon^*/T^*$ are common for the two systems. This implies that the difference in Σ at given $\rho^*_{cg}$ between water and the LJ solvent is caused by difference in structure of the solvent with its interface. The next question is in what way the structure differs from each other. The viewpoint of the test-particle insertion suggests that there are two different aspects of the solvent structure that may affect the local solubility. The first is the probability of forming a sufficiently large cavity that can accommodate a solute molecule. Note that the Boltzmann factor in Eq. (6) is essentially 0 if the repulsive core of a test particle overlaps with any one of repulsive cores of the solvent molecules. The second is the coordination number of solvent molecules around such cavities. The greater the number of solvent molecules in the first solvation shell, the lower the potential energy $\Psi$ in Eq. (6) between the test particle and solvent molecules.

Here we focus on the probability of cavity formation by calculating the local solubility of hard-sphere solutes in water and in the LJ solvent, both with their liquid–vapor interfaces. The solute–solvent interaction potential $\phi_{HS}(r)$ is now

$$\phi_{HS}(r) = \begin{cases} +\infty & (r < d) \\ 0 & (r \geq d). \end{cases} \tag{7}$$

The center of the solute molecule cannot be in any one of the exclusion spheres — the spheres of radius $d$ centered at solvent particles. The solubility Σ of the hard-sphere solute is equal to the probability that the center of the test particle is not included in any one of the exclusion spheres:

$$\Sigma = \frac{V - V_{ex}}{V}, \tag{8}$$

where $V - V_{ex}$ is the volume not covered by any exclusion spheres and $V_{ex}$ is called the excluded volume. In particular, if $d$ is smaller than half

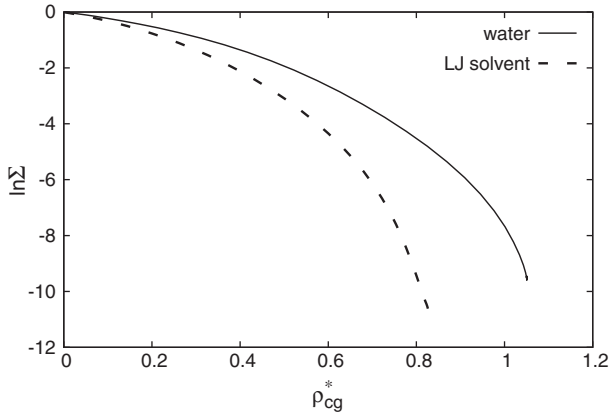


**Fig. 4.** Correlation between ln Σ of the hard-sphere solute with $d^* = 1$ and the reduced coarse-grained density $\rho^*_{cg}$ for water (solid line) and for the LJ solvent (dashed line). The local density of the solvent is coarse-grained over $[z^* - d^*, z^* + d^*]$.

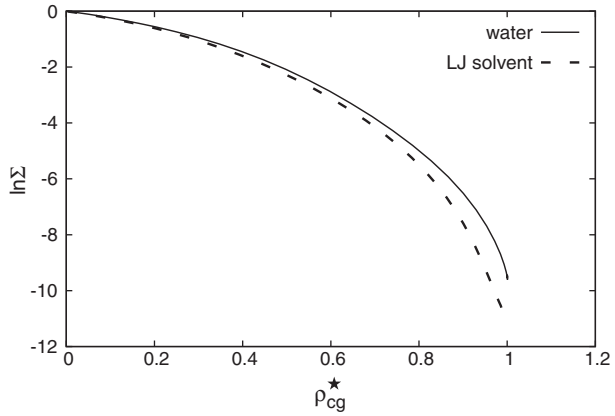


**Fig. 5.** Correlation between ln Σ of the hard-sphere solute with $d^* = 1.0$ and the scaled coarse-grained solvent density $\rho^{\star}_{cg} = \rho_{cg}/\rho^{l}_{B}$ for water (solid line) and for the LJ solvent (dashed line), where $\rho^{l}_{B}$ is the bulk liquid density of each solvent.

the contact distance $d_{BB}$ between solvent molecules, then $V_{ex}$ is $N$ times the volume of each exclusion sphere and

$$\Sigma = 1-(4/3)\pi d^3\rho_B. \tag{9}$$

That is, Σ is a function of $\rho_B$ alone and is independent of the solvent structure. The condition $d < d_{BB}/2$ is, however, unrealistic since the center of a solute particle may even penetrate into the repulsion core of a solvent molecule. Thus, we now consider the case $d > d_{BB}/2$, where difference in solvent structure does matter in determining Σ of hard-spheres.

For inhomogeneous systems with a liquid–vapor interface, Σ of a hard-sphere depends on $z$ and cannot be evaluated from Eq. (8). The local solubility $\Sigma(z)$ is then given by

$$\Sigma(z) = \frac{A-A_{ex}(z)}{A}, \tag{10}$$

where $A$ is the area of the $x$–$y$ plane at $z$ and $A_{ex}(z)$ is the area of the intersection of the $x$–$y$ plane and the exclusion spheres.

In the following paragraph, we examine the correlation between $\Sigma(z^*)$ and $\rho^*_{cg} = \rho_{cg}\sigma^3_{BB}$, the reduced coarse-grained solvent density with $\Delta z^* = d^*$. The values of $d^* = d/\sigma_{BB}$ are chosen to be common between the two solvents. The solvent–solvent contact distance $d_{BB}$ is defined as the distance that for any $r < d_{BB}$, the solvent–solvent radial distribution function in the bulk liquid is zero. We find $d^*_{BB} = d_{BB}/\sigma_{BB} = 0.78$ for water and $d^*_{BB} = 0.92$ for the LJ solvent. For the two solvents, the overlapping of the exclusion spheres may occur when $d^* = 1.0$. We do not consider $d^* < 0.39$ for water and $d^* < 0.46$ for the LJ solvent, for then Σ is expected to be a function of $\rho^*_{cg}$ alone.

In Fig. 4, the local solubility Σ of the hard-sphere solute with $d^* = 1.0$ in water and that in the LJ solvent are given as functions of $\rho^*_{cg}$. For all values of $\rho^*_{cg}$ the solubility of hard-sphere in water is greater than that in the LJ solvent. The same behavior is found for other values of $d^*$ (= 0.6, 0.7, …, 2.0). That the reduced intermolecular distance $r_c/\sigma_{BB}$ of the first peak in the solvent–solvent radial distribution function for water is shorter than that for the LJ solvent is consistent with the present result, since the shorter $r_c/\sigma_{mBB}$, the larger the overlapping volume of the exclusion spheres and the smaller the excluded volume. Recall that when the structure of solvent is the only difference between the two systems with common $\rho_{cg^*}$, the solubility of the LJ solute in water is higher than that in the LJ solvent (Section 4.2). This is now partly explained by the fact that the probability of cavity formation in water is higher than that in the LJ solvent.

### *4.4. Universality in the probability of cavity formation against a scaled density of the solvent*

In the previous section, we have seen that for a given $d^*$ ($> d^*_{BB}/2$), the probability of cavity formation Σ in water is greater than that in the LJ solvent, provided that the reduced coarse-grained solvent density $\rho^*_{cg}$ is common for the two solvents (Fig. 4). Now, we examine the dependence of Σ on a scaled coarse-grained density of the solvent $\rho^{\star}_{cg} = \rho_{cg}/\rho^{l}_{B}$, where $\rho^{l}_{B}$ is the bulk liquid density of the solvent. Plotted in Fig. 5 is ln Σ of the hard-sphere solute with $d^* = 1.0$ for water and that for the LJ solvent against the scaled density $\rho^{\star}_{cg}$. The ln Σ vs $\rho^{\star}_{cg}$ curves for the two solvents are much closer to each other than the ln Σ vs $\rho^*_{cg}$ curves in Fig. 4. We propose that for a given $d^*$ ($> d^*_{BB}/2$), the probability of forming the cavity in the liquid–vapor interface might be a universal function of the scaled coarse-grained density of the solvent $\rho^{\star}_{cg}$. At least, from the present study, the universality is observed for the liquid–vapor interface of water and that of simple fluids, when they are close to the triple point.

## Acknowledgment

We thank Dr. T. Sumi, Dr. R. Roth, and Dr. T. Yagasaki for helpful discussions and comments. This work is supported by a Grant-in-Aid for Scientific Research and the program for promoting the enhancement of research universities from MEXT, Japan.

## References

[1] V.M. Kaganer, H. Möhwald, P. Dutta, Rev. Mod. Phys. 71 (1999) 779.
[2] K.B. Eisenthal, Chem. Rev. 96 (1996) 1343.
[3] G.L. Richmond, Chem. Rev. 102 (2002) 2693.
[4] P. Jungwirth, D.J. Tobias, Chem. Rev. 106 (2006) 1259.
[5] I. Benjamin, Acc. Chem. Res. 28 (1995) 233.
[6] B.C. Garrett, G.K. Schenter, A. Morita, Chem. Rev. 106 (2006) 1355.
[7] T.M. Chang, L.X. Dang, Chem. Rev. 106 (2006) 1305.
[8] L.R. Pratt, A. Pohorille, Chem. Rev. 102 (2002) 2671.
[9] Y.R. Shen, Nature 337 (1989) 519.
[10] J.M. Hicks, K. Kemnitz, K.B. Eisenthal, T.F. Heinz, J. Phys. Chem. 90 (1986) 560.
[11] D.J. Donaldson, J.A. Guest, M.C. Goh, J. Phys. Chem. 99 (1995) 9313.
[12] T.L. Tarbuck, G.L. Richmond, J. Am. Chem. Soc. 127 (2005) 16806.
[13] T.L. Tarbuck, G.L. Richmond, J. Am. Chem. Soc. 128 (2006) 3256.
[14] G. Ma, H.C. Allen, Langmuir 22 (2006) 5341.
[15] Th. Rasing, Y.R. Shen, M.W. Kim, P. Valint Jr., J. Bock, Phys. Rev. A 31 (1985) 537.
[16] E. Tyrode, C.M. Johnson, A. Kumpulainen, M.W. Rutland, P.M. Claesson, J. Am. Chem. Soc. 127 (2005) 16848.
[17] I. Benjamin, Chem. Rev. 96 (1996) 1449.
[18] A. Pohorille, I. Benjamin, J. Chem. Phys. 94 (1991) 5599.
[19] P. Jedlovszky, I. Varga, T. Gilányi, J. Chem. Phys. 119 (2003) 1731.
[20] L.B. Pártay, P. Jedlovszky, P.N.M. Hoang, S. Picaud, M. Mezei, J. Phys. Chem. C 111 (2007) 9407.
[21] R. Vácha, P. Slavíček, M. Mucha, B.J. Finlayson-Pitts, P. Jungwirth, J. Phys. Chem. A 108 (2004) 11573.
[22] R. Vácha, P. Jungwirth, J. Chen, K. Valsaraj, Phys. Chem. Chem. Phys. 8 (2006) 4461.
[23] R.S. Taylor, D. Ray, B.C. Garrett, J. Phys. Chem. B 101 (1997) 5473.
[24] A.J. Howes, C.J. Radke, Langmuir 23 (2007) 1835.
[25] B. Widom, J. Stat. Phys. 19 (1978) 563.
[26] B. Widom, J. Phys. Chem. 86 (1982) 869.
[27] J.S. Rowlinson, B. Widom, Molecular Theory of Capillarity, Dover Publications, New York, 2002. p. 82.
[28] J.O. Hirschfelder, C.F. Curtiss, R.B. Bird, Molecular Theory of Gases and Liquids, Wiley, New York, 1954.
[29] J.L.F. Abascal, C. Vega, J. Chem. Phys. 123 (2005) 234505.
[30] C. Ibergay, A. Ghoufi, F. Goujon, P. Ungerer, A. Boutin, B. Rousseau, P. Malfreyt, Phys. Rev. E 75 (2007) 051602.
[31] A. Pohorille, M.A. Wilson, J. Chem. Phys. 104 (1996) 3760.
[32] H.A. Patel, E.B. Nauman, S. Garde, J. Chem. Phys. 119 (2003) 9199.
[33] J.S. Rowlinson, B. Widom, Molecular Theory of Capillarity, Dover Publications, New York, 2002. p. 31.
[34] B. Hess, C. Kutzner, D. van der Spoel, E. Lindahl, J. Chem. Theory Comput. 4 (2008) 435.
[35] S. Nosé, J. Chem. Phys. 81 (1984) 511.
[36] S. Nosé, Mol. Phys. 52 (1984) 255.
[37] W.G. Hoover, Phys. Rev. A 31 (1985) 1695.